Scientific Journal of Impact Factor (SJIF): 5.71

e-ISSN (O): 2348-4470
p-ISSN (P): 2348-6406

International Journal of Advance Engineering and Research Development

Volume 6, Issue 04, April -2019

REVIEW OF MODEL BASED PREDICTIVE CONTROL STRATEGY FOR PERMANENT MAGNET SYNCHRONOUS GENERATOR BASED WIND TURBINE SYSTEM

[1]Pravin Garg, [2]Shri Rakesh Sharma

[1]*Student M. Tech (PS&C) BBDU, Lucknow.*
[2]*Astt. Proff. BBDU, Lucknow.*

ABSTRACT: *This review paper reviews a **Model Predictive Control** (**MPC**) strategy for **Permanent Magnet Synchronous Generator** (**PMSG**) based **Variable Speed-Wind Energy Conversion System** (**VS-WECS**). For extraction of maximum power from wind turbine, a 3-ϕ **back-to-back** (**BTB**) **converter is** used to tie P**MSG** and **grid** with **L-filter**. Control algorithm is applied to **Machine side Converter** (**MSC**) to obtain the maximum power from the **WECS**. Similarly, Control algorithm is applied to **Grid side Converter** (**GSC**) to obtain dc-link voltage regulation.*

*Model of variable-speed WECS having directly driven PMSG is developed in **MATLAB/ SIMULINK** environment. Good dynamic performance of WESC under wind speed variation is achieved using MPC. Validation of the effectiveness of proposed control approach is seen in MATLAB enviournment.*

MPC controlled model of the converter based WECS allows foreseeing the predicted behavior of the controlled variables. This allows selection of the voltage vector that leads to minimization of error, by minimizing a predefined cost function to produce firing pulse for running of convertors. The robustness of system alongwith low current THD is main feature of proposed scheme. Simulation results in Matlab-Simulink software environment gives out the performances of the Model Predictive control strategy.

1. Introduction

Increase in demand for electrical energy, depletion of Hydrocarbon, ever increasing cost of electrical energy from the fossil based generation are the main cause to move towards renewable energy systems. The awareness/ efforts on reducing pollution/ carbon foot print have further pushed to go for renewable energy systems in last decade.

In order to give greener and cleaner energy from the available options of renewable energy systems, wind energy systems has come out as a promising option. Various options are available in WESC's. These various WESC configurations are based on variation of wind speed based on usage of windmill with or without gear having various available choice of generator's.

Among different generators the use of Permanent Magnet Generator has come out as most promising and successful configuration due to high power density, high degree of precision, variable speed operation, lesser maintenance, increased reliability due to absence of gear boxes and good grid compatibility [5]. In proposed VS-WECS system PMSG is directly coupled with WT with its stator windings tied to grid through a BTB full scale converter.

Implementation of advanced control schemes enhances the performance of VS-WECS. Among various schemes available, model predictive control (MPC) is found to be easily implementable [6] and effective. In MPC schemes, system model is used to predict the future behavior of the controlled variables. Controlled variable based cost function is used to select the voltage vector, which minimizes the error between the controlled and its reference variable. MPC can be used in variety of systems having different contrarians. Nonlinearities and multi-variable controlled parameter can easily be included in this scheme as its own prediction guides the next step of controlling.

Mechanical power output of WT changes with the change in wind speed. MPPT algorithms are used to maintain maximum mechanical power during variation in wind speed. PMSG is tied to the grid via a 3ϕ back-to-back (BTB) converter with L-filter. Between the two converters a shunt capacitor acts as dc-link. Two MPC based control schemes are developed for machine and grid side converters. MPC scheme of Machine Side Controller is to draw maximum power. MPC scheme for Grid Side Convertor is to control active power transferred to the grid. Tip speed

ratio (**TSR/ λ**) algorithm is used to maintain the mechanical power to its optimal value. For ease of understanding, this paper is subdivided in following sections:-

(a) Section 2 discusses the WECS system modeling.
(b) Section 3discusses Application of MPPT technique.
(c) Control of the MSC and GSC is discussed in section 4.
(d) The principles of MPC for MSC and GSC are discussed in section 5.
(e) The system results are given in section 6.
(f) Conclusions is in section 7.

2. Mathematical Modeling of Wind Energy Conversion System

This section discusses the WECS having a three-phase PMSG and a 3-ϕ BTB converter connected to grid as shown in Fig. 1.

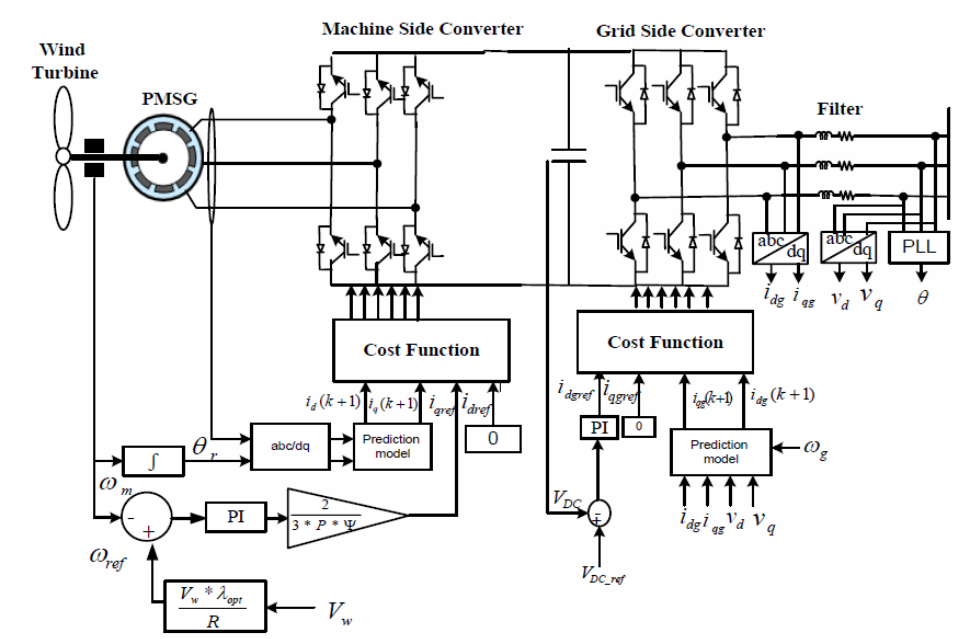

Fig. 1. Proposed MPC Controlled PMSG based WECS Configuration

2.1 Mathematical modeling of WT

On wind application, turbine rotates at certain speed; kinetic energy of wind generates the mechanical power, which drives the permanent magnet synchronous generator. For a wind turbine, the output mechanical power and torque generated can be defined as:

$$\mathbf{Pm} = \frac{1}{2}\boldsymbol{\rho}\mathbf{ACp}(\boldsymbol{\lambda},\boldsymbol{\beta})*\mathbf{v}^3_{\mathbf{w}} \quad \text{Eq.(1)}$$

$$\mathbf{T_m} = \mathbf{P_m}/\ \boldsymbol{\omega}_{\mathbf{m}} \quad \text{Eq.(2)}$$

Where, $\mathbf{P_m}$ is turbine output (Watts), $\mathbf{T_m}$ is mechanical torque (Nm), $\mathbf{C_p}$ is dimensionless turbine power coefficient, $\boldsymbol{\rho}$ is the air density (kg/m^3), **A** is the area swept by the turbine blades (m$^{2)}$, $\mathbf{V_w}$ is the wind velocity (m/s), and $\boldsymbol{\omega}_{\mathbf{m}}$ is the mechanical angular speed of the turbine(rad/ sec).

The power extraction efficiency or turbine power coefficients $\mathbf{C_p}$ is a nonlinear function of tip speed ratio $\boldsymbol{\lambda}$ and the blade pitch angle $\boldsymbol{\beta}$. The tip speed ratio $\boldsymbol{\lambda}$ is a variable, which expresses the ratio of the linear speed of the tip of blades to rotational speed of WT, as follows:

$$\boldsymbol{\lambda} = \boldsymbol{\omega}_{\mathbf{m}}\mathbf{R}/\ \mathbf{V_w} \quad \text{Eq.(3)}$$

Where, R is the radius of the turbine blade.

Here, C_p is defined as function of **λ** and **β** as follows:

$$C_p(\lambda,\beta) = C_1 (C_2/\lambda_1 - C_3\beta - C_4)\, e^{-C5/\lambda 1} + C_6\, \lambda \qquad \text{Eq.(4)}$$

Where, $$1/\lambda_1 = 1/(\lambda + 0.08\,\beta) - 0.035/(1+\beta^2) \qquad \text{Eq.(5)}$$

The relation between C_p and **λ (at β = 0^0)** is given in Fig. 2.

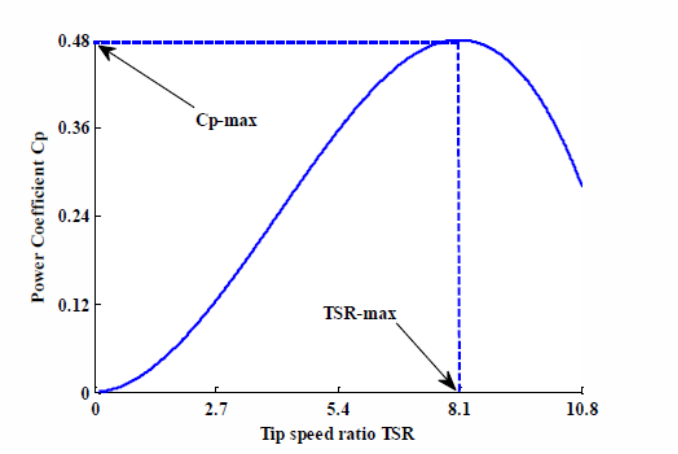

Fig. 2. Power Coefficient (C_p) vs. Tip Speed Ratio (TSR/ λ)

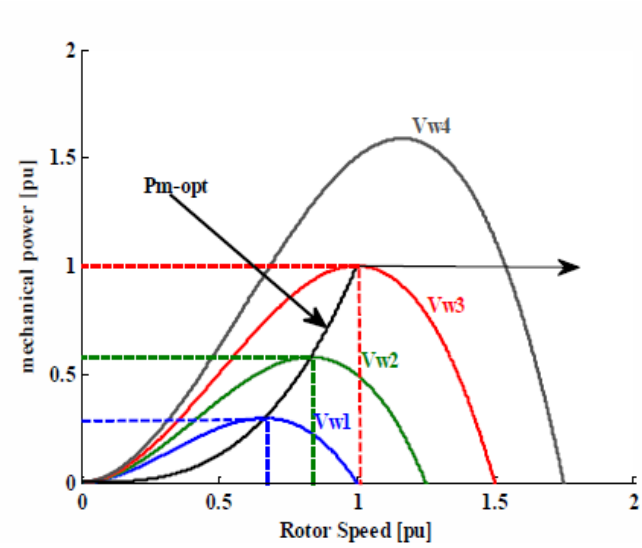

Fig. 3. Generated Mechanical Power vs. Rotor Speed at different Wind Speed

2.2 Mathematical modeling of Permanent Magnet Synchronous Generator (PMSG)

2.2.1 Voltage equations of a three-phase PMSG in the rotor reference frame (using an extended Park transformation) can be defined as:

$$V_{ds} = R_s\, i_{ds} - \omega_r\, \psi_{qs} = R_s\, i_{ds} - \omega_r\, L_{qs}\, i_{qs} \qquad \text{Eq.(6)}$$

$$V_{qs} = R_s\, i_{qs} + \omega_r\, \psi_{ds} = R_s\, i_{qs} + \omega_r\, L_{ds}\, i_{ds} + \omega_r\, \psi_r \qquad \text{Eq.(7)}$$

Where $\mathbf{V_{ds}}$/ $\mathbf{V_{qs}}$ and $\mathbf{i_{ds}}$/ $\mathbf{i_{qs}}$ refers to the stator voltages/ currents (both in d, q axis), $\mathbf{R_s}$ is stator resistance, $\mathbf{L_{ds}}$, $\mathbf{L_{qs}}$ are the (d, q) axis inductances.

$\omega_e = p_p \omega_r$,

Where $\mathbf{p_p}$ is pole pairs, $\boldsymbol{\omega_m}$ is turbine rotor angular speed and $\boldsymbol{\psi_s}$ is the permanent flux linkage.

Electromagnetic torque of the PMSG can be expressed as:

$$T_e = 3/2\, p_p\, \psi_s\, i_s \qquad \text{Eq.(8)}$$

The relation between mechanical torque and electromagnetic torque is given by:

$$T_m = T_e + f\,\omega_m + Jd\,\omega_m/dt \qquad \text{Eq.(9)}$$

Where **f** is friction coefficient, **J** is moment of inertia.

2.2.1 Steady state dq-axis stator flux linkage

The flux equations for 3-ϕ PMSG in rotor reference frame (using an extended Park transformation) can be defined as:

$$\psi_{ds} = L_{ds}\, i_{ds} + \psi_r \text{ and } \qquad \psi_{qs} = L_{qs}\, i_{qs} \qquad \text{Eq.(10)}$$

2.2.2 Stator Power Output

The power (real, reactive and apparent) equations of a three-phase PMSG is expressed in the rotor reference frame using an extended Park transformation are as follows:

$$P_s = 3\, V_s\, I_s \cos\varphi_s = 1.5\,(V_{ds}\, i_{ds} + V_{qs}\, i_{qs}) \qquad \text{Eq.(11)}$$

$$Q_s = 3\, V_s\, I_s \sin\varphi_s = 1.5\,(V_{qs}\, i_{ds} - V_{ds}\, i_{qs}) \qquad \text{Eq.(12)}$$

$$S_s = 3\, V_s\, I_s = (P^2_s + Q^2_s)^{1/2} \qquad \text{Eq.(13)}$$

3. Maximum Power Point Tracking Technique (MPPT)

MPPT techniques are used to maintained mechanical power to its maximum/ optimal value during different wind speed conditions. Among various available techniques, the **Tip Speed Ratio** (**TSR**) technique (for adjusting the rotor speed to its optimum values at different wind speeds to achieve maximum power output) is used in this scheme. This technique is based on measuring the wind and rotor speeds and their comparison to reference rotational speed at different wind speeds. It can be given as:

$$\omega_{ref} = \lambda_{opt}\, R/ V_w \qquad \text{Eq.(14)}$$

Where $\boldsymbol{\omega_{ref}}$ is reference rotor speed, $\boldsymbol{\lambda_{opt}}$ is optimum TSR, R is blade radius and $\mathbf{V_w}$ is wind speed.

Eq. (9) indicates that the **control of generator speed can be achieved by the control of electromagnetic torque**. From **Eq. (8)** the **electromagnetic torque is proportional to the q-axis current of PMSG**, Therefore the rotor speed can be controlled by changing the q-axis current of PMSG.

$$i_{qref} = 2T_m/ 3P_p\, \psi \qquad \text{Eq.(15)}$$

4. Control Strategy for Machine Side and Grid Side Converters

A BTB converter acts as a **rectifier in MSC** and **inverter in GSC**. The MSC adjust the rotor speed to its optimal values at different wind speeds so as to extracts maximum power during wind speed variations fro WT. MSC works in two loops, **outer loop adjust the rotor speed through a PI controller** and the **inner loop is to control d-q axis stator currents to its reference values through a MPC**.

GSC maintains the dc-link capacitor voltage to its reference value and **controls the real and reactive power**. The **inner controls the power** and **outer loop regulates the dc-link capacitor voltage** through PI controllers.

5. Model Predictive Control

The MPC controller predicts/ estimates the upcoming behavior of controlled variables for a limited horizon of time and digitally selects the optimal actuations by minimizing the cost function **g**. Working principles of MPC are given in Fig.4

(a) A model is required for the system to predict the future behavior of controlled variables until a horizon in time is achieved.
(b) A cost function is defined to truly represent the desired behavior of the system.
(c) The optimal actuation is obtained by digital minimizing the cost function.

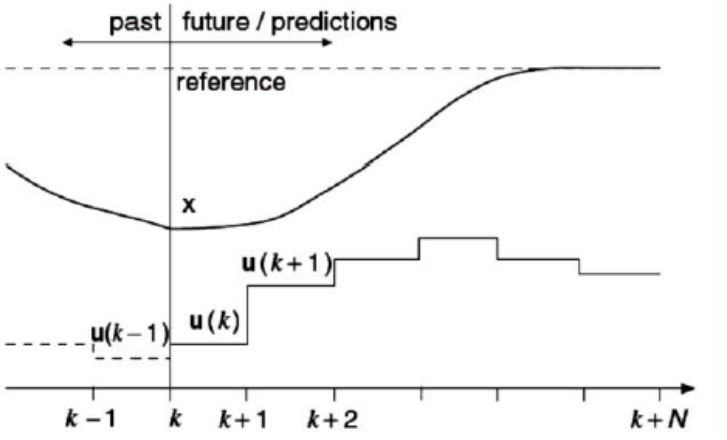

Fig. 4. Basic Principles of MPC

In this review, the MPC technique is used to **extract maximum power at different wind speeds at MSC** (electromagnetic torque controller) and in the **control the reactive power** at **GSC**.

5.1 Model Predictive Control of Convertors (GSC/ MSC)

Mathematical model of the GSC connected to the grid through an L filter(d-q synchronous reference frame) can be written as:

$$di_{gd}/dt = 1/L_g\,(V_{gd} - R_g\, i_{gd} + \omega_g\, L_g\, i_{gq} - V_{convd}) \quad \text{Eq.(16)}$$

$$di_{gq}/dt = 1/L_g\,(V_{gq} - R_g\, i_{gq} - \omega_g\, L_g\, i_{gd} - V_{convq}) \quad \text{Eq.(17)}$$

$$P = V_{gd}\, i_{gd} + V_{gq}\, i_{gq} \quad \text{Eq.(18)}$$

$$Q = V_{gq}\, i_{gd} - V_{gd}\, i_{gq} \quad \text{Eq.(19)}$$

Where i_{gd}/ i_{gq} and V_{gd}/ V_{gq} are the d-q components of the grid current/ voltage vectors and ω_g is angular frequency of grid. V_{convd} and V_{convq} are the d-q components of the converter output voltage vector. L_g and R_g respectively are the resistor and inductor of the **L-filter**. di_{gd}/dt and di_{gq}/dt are the time derivatives instantaneous grid currents.

On discretisation of stator current with a sampling time Ts, the discrete-time model can be expressed by **forward Euler approximation** of derivatives. The stator current derivative di/ dt is replaced by a Euler approximation and can be written as:

$$di/dt = (i[k+1] - i[k])/T_s \quad \text{Eq.(20)}$$

Therefore, mathematically PMSG equations can also be written as:

$$i_d[k+1] = (1 - T_s R_s/L_d)^* i_d[k] + (T_s L_q/L_d)^* \omega_e * i_q[k] + T_s V_d[k]/L_d \quad \text{Eq.(21)}$$

$$i_q[k+1] = (1 - T_s R_s/L_q)^* i_q[k] - (T_s L_d/L_q)^* \omega_e * i_d[k] + T_s V_q[k]/L_q - T_s \psi\, \omega_e/L_q \quad \text{Eq.(22)}$$

Therefore the cost function, g, can be defined as:

$$g = |[i_{dref}[k+1] - i_d[k+1]]| + |[i_{qref}[k+1] - i_q[k+1]]| \quad \text{Eq.(23)}$$

Where $\mathbf{i_{dref}}$ **[k + 1]** and $\mathbf{i_{qref}}$ **[k + 1]** are the reference values of d-q-axis stator currents at $[k+1]^{th}$ sampling instance. The cost function is estimated for each sampling state and the minimum value of cost function is applied at the next sampling instant as reference.

5.1.1 MPC based control of MSC

MPC-based control scheme for the MSC is given Fig. 5. Converter voltage vector based estimation is required and applied during in next sampling period in order to minimise the error between the stator reference currents (in the dq synchronous reference frame).

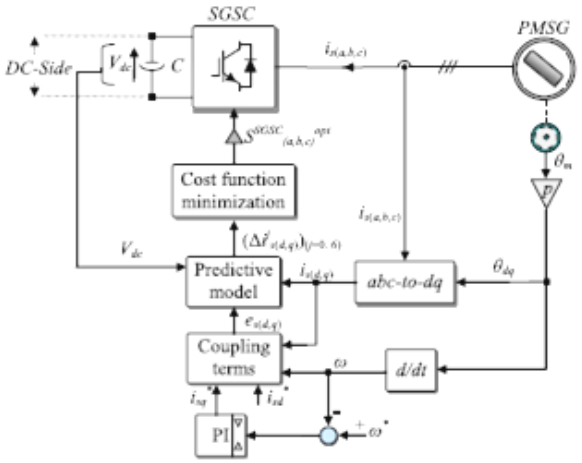

Fig. 5. MPC based control for the MSC/ SGSC

The d axis stator current reference $\mathbf{i_{sd}}$*** is set to zero to obtain the maximum torque at the minimum current**, whereas the q axis stator current reference is q* is computed via PI-based speed controller. Digital predictive current controller algorithm can be developed based on expressions (16) and (17) as under:

$$\mathbf{di_{sd}/dt = 1/L_{sd}(V_{sd} - R_s i_{sd} + \omega_{dq} L_{sq} i_{sq})} \quad \text{Eq.(24)}$$

$$\mathbf{di_{sq}/dt = 1/L_{sd}(V_{sq} - R_s i_{sq} + \omega_{dq} L_{sq} i_{sd} + \omega_{dq}\phi_{rd})} \quad \text{Eq.(25)}$$

By using forward Euler discretisation method, the above equation can be defined as:

$$\mathbf{i_{sd}[k+1] = a_0(V_{sd}[k] - e_{sd}[k]) + a_1 i_{sd}[k]} \quad \text{Eq.(26)}$$

$$\mathbf{i_{sq}(k+1) = a_3(V_{sq}[k] - e_{sq}[k]) + a_3 i_{sq}[k]} \quad \text{Eq.(27)}$$

$$\mathbf{e_{sd}[k] = - L_{sq}\, \omega_{dq}[k] i_{sq}[k]} \quad \text{Eq.(28)}$$

$$\mathbf{e_{sq}[k] = L_{sd}\, \omega_{dq}[k] i_{sd}[k] + \omega_{dq}[k]\, \phi_{rd}[k]} \quad \text{Eq.(29)}$$

Where,

$$\mathbf{a_0 = T_s/ L_{sd}}$$
$$\mathbf{a_1 = 1 - R_s\, T_s/ L_{sd}} \quad \text{Eq.(30)}$$
$$\mathbf{a2 = T_s/ L_{sq}}$$
$$\mathbf{a3 = - (1 - R_s\, T_s/ L_{sq})}$$

And Ts is the sampling period. $\mathbf{i_{sd}[k+1]}$ and $\mathbf{i_{sq}[k+1]}$ (respectively $\mathbf{i_{sd}[k]}$ and $\mathbf{i_{sq}[k]}$) are the predicted d-q stator current components at the $(k+1)^{th}$ and k^{th} sampling period.

The **esd** and **esq** refer respectively to the d- q induced EMF terms. During each sampling period, the **evolution of the d-q stator current components depends on the applied stator voltage components** $\mathbf{V^j_{sd}[k]}$ and $\mathbf{V^j_{sq}[k]}$ at the kth sampling period. These stator voltage components expressed in the d-q synchronous reference frame and can be obtained by rotation operation of an angle equal to $\boldsymbol{\theta_{dq}}$ to the **αβ** components of the stator voltage vectors as shown in matrix form:-

$$\mathbf{[V^j_{sd}[k], V^j_{sq}[k]] = [\cos(\theta_{dq}[k]), \sin(\theta_{dq}[k]), -\sin(\theta_{dq}[k]), \cos(\theta_{dq}[k])] * [V^j_{s\alpha}[k], V^j_{s\beta}[k]]} \quad \text{Eq.(31)}$$

Eight switching states combinations of the MSC with two combinations that lead to null stator voltage vector are given in Table. 1.

Table. 1. MSC switching states and corresponding output voltage vector $V^{j}_{sdq(j=0to7)}$

S_{sa}	S_{sb}	S_{sc}	$V^{j}_{s\alpha}$	$V^{j}_{s\beta}$	Vector V^{j}	Vector V^{j}_{sdq}
0	0	0	0	0	V_0	V^{0}_{sdq}
1	0	0	$2V_{dc}/3$	0	V_1	V^{1}_{sdq}
1	1	0	$V_{dc}/3$	$V_{dc}/\sqrt{3}$	V_2	V^{2}_{sdq}
0	1	0	$-V_{dc}/3$	$V_{dc}/\sqrt{3}$	V_3	V^{3}_{sdq}
0	1	1	$-2V_{dc}/3$	0	V_4	V^{4}_{sdq}
0	0	1	$-V_{dc}/3$	$-V_{dc}/\sqrt{3}$	V_5	V^{5}_{sdq}
1	0	1	$V_{dc}/3$	$-V_{dc}/\sqrt{3}$	V_6	V^{6}_{sdq}
1	1	1	0	0	V_7	V^{7}_{sdq}

Stator d-q axis currents can be defined for the different possibilities of the d-q stator voltage components $V^{j}_{sd}[k]$ and $V^{j}_{sq}[k]$ of the voltage vectors V^{j}_{sdq} as under:

$$\{i^{j}_{sd}[k+1] = a_0(V^{j}_{sd}[k] - e_{sd}[k]) + a_1 i_{sd}[k]\} \quad \{\text{for } j = 0 \text{ to } 7\} \quad \text{Eq.(32)}$$

$$\{i^{j}_{sq}[k+1] = a_3(V^{j}_{sq}[k] - e_{sq}[k]) + a_4 i_{sq}[k]\} \quad \{\text{for } j = 0 \text{ to } 7\} \quad \text{Eq.(33)}$$

Where $\mathbf{i^{j}_{sd}[k+1]}_{(j=0to7)}$ and $\mathbf{i^{j}_{sq}[k+1]}_{(j=0to7)}$ are the predicted d-q stator current components at the $(k+1)^{th}$ sampling period when the $\mathbf{(V^{j}_{s\alpha}[k])}^{(j=0to7)}$ and $\mathbf{(V^{j}_{s\alpha}[k])}^{(j=0to7)}$ voltage vector components are applied during the k^{th} sampling period.

It is possible to predict the d-q stator vector components $(\Delta\, \mathbf{i^{j}_{sd}[k+1]})^{(j=0to7)}$ and $(\Delta\, \mathbf{i^{j}_{sq}[k+1]})^{(j=0to7)}$. This current errors are defined as the difference between the reference stator current vector at the k^{th} sampling period and the predicted one at the $(k+1)^{th}$ sampling period when the stator voltage vector $\mathbf{V^{j}_{sdq}[k]}^{(j=0to7)}$ is applied.

Therefore, we can say:

$$\Delta\, \mathbf{i^{j}_{sd}[k+1]}_{(j=0to7)} = \mathbf{i^{*}_{sd}[k] - i^{j}_{sd}[k+1]}^{(j=0to7)} \quad \text{Eq.(34)}$$

$$\Delta\, \mathbf{i^{j}_{sq}[k+1]}_{(j=0to7)} = \mathbf{i^{*}_{sq}[k] - i^{j}_{sq}[k+1]}^{(j=0to7)} \quad \text{Eq.(35)}$$

Similarly a cost function g_s can be defined based on various equations discussed above in Eqn (24) to (33). It is applied to the obtained stator current error components. This cost function is given in Eq. (36).

$$\{\mathbf{g_s^{j}} = |(\Delta\, \mathbf{i^{j}_{sd}[k+1]}| + |\Delta\, \mathbf{i^{j}_{sq}[k+1])}|\}_{(j=0to7)} \quad \text{Eq.(36)}$$

Finally, an optimization procedure is adopted. This procedure contains selecting the optimal switching states combination $S_{opt(a,b,c)}^{SGSC\ opt}$ that results in the minimal cost function Min $\mathbf{g_s^{j}}_{(j=0to7)}$ at which convertor fires.

5.1.2 MPC based control of GSC

The MPC based control for the GSC is given at Fig. 6. The main aim of the MPC algorithm for the GSC is to control the active and reactive power. This is obtained through the control of d-q grid current components. The d axis grid current reference $\mathbf{i_{gd}^{*}}$ is estimated by the PI controller of the outer dc-link voltage control loop, whereas the q axis grid current reference $\mathbf{i_{gd}^{*}}$ is set to zero in order to achieve a unit power factor operation.

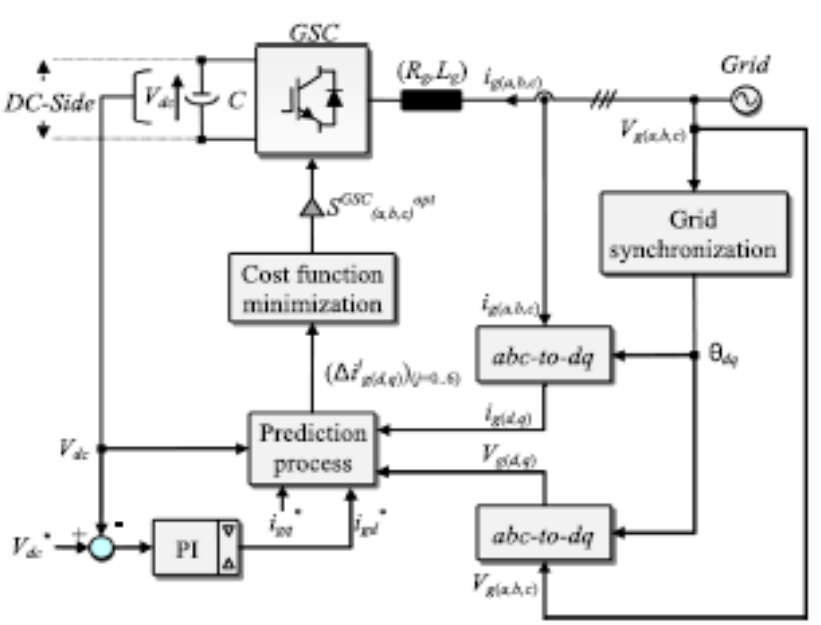

Fig. 6. MPC based control for the GSC

Digital predictive current controller algorithm can be developed based on expressions (16) (17) (26) and (27) as under:

$$\mathbf{I_{gd}[k+1] = b_0(V_{gd}[k] - V_{convd}[k]) + b_2 i_{gq}[k]} \quad \text{Eq.(37)}$$

$$\mathbf{I_{gq}[k+1] = b_0(V_{gq}[k] - V_{convd}[k]) + b_1 i_{gq}[k] - b_2 i_{gd}[k]} \quad \text{Eq.(38)}$$

Where, Ts is the sampling period and

$$\mathbf{b_0 = T_s/L_g}$$
$$\mathbf{b_1 = (1 - R_g T_s/ L_g)} \quad \text{Eq.(39)}$$
$$\mathbf{b_2 = \omega_g T_s\, igd[k+1]}$$

Where $\mathbf{i_{gd}[k+1]/\ i_{gq}[k+1]}$ are the predicted d-q grid current components at the $(k+1)^{th}$ sampling period. During sampling period, evolution of d-q grid current components depends on the applied converter voltage components $\mathbf{V_{convd}[k]}$ and $\mathbf{V_{convq}[k]}$ at the k^{th} sampling period.

The voltage vectors $\mathbf{V^j_{convd}[k]}$ and $\mathbf{V^j_{convq}[k]}$ depend also on the dc-link voltage $\mathbf{V_{dc}}$ level as shown in Eqs. (37) and (38). For simplification reasons the dc-link voltage is supposed equal to its reference $\mathbf{V_{dc}^*}$. Therefore,

$$\mathbf{[V^j_{convd}[k], V^j_{convq}[k]]=[cos(\theta_{dq}[k]), sin(\theta_{dq}[k]), - sin(\theta_{dq}[k]), cos(\theta_{dq}[k])] [V^j_{conv\alpha}[k], V^j_{conv\beta}[k]]} \quad \text{Eq.(40)}$$

$$\mathbf{[V^j_{conv\alpha}[k], V^j_{conv\beta}[k]] = 2/3V^*_{dc}[1, -1/2, -1/2, 0, \sqrt{3}/2, -\sqrt{3}/2] *[S_{ia}[k], S_{ib}[k], S_{ic}[k]]} \quad \text{Eq.(41)}$$

Where $\mathbf{V^j_{conv\alpha}[k]}$ and $\mathbf{V^j_{conv\beta}[k]}$ are the output converter voltage vectors in the stationary αβ coordinates, and $S_{(a,b,c)}^{GSC}[k]$ are the switching signals of the GSC.

The number of switching states combinations is equal to eight with two combinations that lead to null converter voltage vector. Eqs. (26) and (27) can be expressed for the different possibilities of the d-q converter voltage components $V^j_{convd}[k]$ and $V^j_{convq}[k]$ of the voltage vectors $V^j_{convdq}[k]$ as follows:

$$\mathbf{\{i^j_{gd}[k+1] = a_0(V_{gd}[k] - V^j_{convd}[k]) + a_1 i_{gd}[k]) + a_2 i_{gq}[k]\}} \quad \mathbf{\{for\ j=0\ to\ 7\}} \quad \text{Eq.(42)}$$

$$\mathbf{\{i^j_{gq}[k+1] = a_3(V_{gq}[k] - V^j_{convd}[k]) + a_1 i_{gq}[k]) - a_2 i_{gd}[k]\}} \quad \mathbf{\{for\ j=0\ to\ 7\}} \quad \text{Eq.(43)}$$

Table. 2. GSC switching states and corresponding output voltage vector $V^{j}_{convdq(j=0to7)}$

S_{ia}	S_{ib}	S_{ic}	$V^{j}_{conv\alpha}$	$V^{j}_{conv\beta}$	Vector V^{j}	Vector V^{j}_{convdq}
0	0	0	0	0	V_0	V^{0}_{sdq}
1	0	0	$2V_{dc}/3$	0	V_1	V^{1}_{sdq}
1	1	0	$V_{dc}/3$	$V_{dc}/\sqrt{3}$	V_2	V^{2}_{sdq}
0	1	0	$-V_{dc}/3$	$V_{dc}/\sqrt{3}$	V_3	V^{3}_{sdq}
0	1	1	$-2V_{dc}/3$	0	V_4	V^{4}_{sdq}
0	0	1	$-V_{dc}/3$	$-V_{dc}/\sqrt{3}$	V_5	V^{5}_{sdq}
1	0	1	$V_{dc}/3$	$-V_{dc}/\sqrt{3}$	V_6	V^{6}_{sdq}
1	1	1	0	0	V_7	V^{7}_{sdq}

where $(\mathbf{i^{j}_{gd}[k+1]})^{(j=0to7)}$ and $(\mathbf{i^{j}_{gq}[k+1]})^{(j=0to7)}$are the predicted d- q grid current components at the$(k+1)^{th}$ sampling period, when the$(\mathbf{V^{j}_{conv\alpha}[k]})^{(j=0to7)}$) and $(\mathbf{V^{j}_{conv\beta}[k]})^{(j=0to7)}$) voltage vector components are applied during the k^{th} sampling period. It is possible to firstly predict the **d-q grid current error vector components vector** $(\mathbf{\Delta i^{j}_{gd}[k+1]})^{(j=0to7)}$ and $(\mathbf{\Delta i^{j}_{gq}[k+1]})^{(j=0to7)}$. These errors are defined as the difference between the reference grid current vector at the k^{th} sampling period and the predicted one at sampling period $(k+1)^{th}$ when the converter voltage vector$(V^{j}_{convdq}[k])^{(j=0to7)}$ is applied. The grid current error vector components are expressed as in (44) and (45).

$$(\mathbf{\Delta i^{j}_{gd}[k+1] = i^{*}_{gd}[k] - i^{j}_{gd}[k+1]})^{(j=0to7)} \quad \text{Eq.(44)}$$

$$(\mathbf{\Delta i^{j}_{gq}[k+1] = i^{*}_{gq}[k] - i^{j}_{gq}[k+1]})^{(j=0to7)} \quad \text{Eq.(45)}$$

Based on relations (42), (43), (44) and (45), a cost function gi is obtained as grid current error components. This cost function is defined in Eq. (46).

$$\{\mathbf{g^{j}_{i} = |\Delta i^{j}_{gd}[k+1]| + |\Delta i^{j}_{gq}[k+1]|}\}^{(j=0to7)} \quad \text{Eq.(46)}$$

Finally, an optimization procedure is adopted. This procedure contains selecting the optimal switching states combination $S_{opt(a,b,c)}$ SGSC opt that results in the minimal cost function Min $\mathbf{g_s^{j}}_{(j=0to7)}$ at which convertor fires.

5.2 The essence of the model predictive algorithm is the cost function minimization [24, 25]. This process consists of selecting the optimal switching signals $S^{GSC}{}_{(a,b,c)}{}^{opt}$ that lead to the minimal cost function $Min(g_i^{j})^{(j=0to7)}$.

6. SIMULATION RESULTS

Effectiveness and Validity of the system is verified in Matlab/Simulink enviournment. Parameters of the system under study are as under:

Table. 3. Simulation Parameters

Parameter	Value	Parameter	Value
DC Link Capacitor C	2000μF/ 800V	**Pole Pair**	5
DC Link Reference Voltage V^{*}_{dc}	600V	**Ts**	40μS
Initial DC Link Voltage	560V	**Flux Linkage ψ**	0.433Wb
I^{*}_{sd} Reference(Stator)	0 for Max Torque	**Speed reference PMSG ω^{*}**	250Rad/ sec
I^{*}_{gd} Reference(Grid)	0 for Unit PF	**Grid Frequency**	50Hz
Ld	0.00835H	**Moment of Inertia (J)**	0.01197 kgm^2
Lq	0.00835H	**Blade Radius**	1.8m
Lg(Grid Inductance)	50mH/ 20A	**Air Density**	1.225Kg/m^3
Filter Inductance Lg	0.002H	**Optimal Tip Speed Ratio**	8.1
Rg(Grid Resistance)	0.015 Ω	**Max Power Coeffiecient**	0.48
Filter Resistance Rg	3Ω	**No Switching States**	08
Stator resistance Rs	0.425 Ω		

Fig. 5 represents the actual wind speed at which measured and reference generator speed, actual and maximum mechanical power, the turbine's power coefficient, the turbine tip speed ratio (TSR) with electromagnetic torque of the PMSG are shown (Wind speed profile varies up and down as a step function with mean wind speed of 12 m/sec).

MPC scheme controlled controller gives a good tracking of the actual/ reference values of the rotor speed. The difference between electrical and mechanical powers is found out to be very small. The system operates at the optimal power coefficient value (0.48). The tip speed ratio reaches maximum value (8.1). The turbine torque T_m and generator torque T_e are coinciding well.

Fig. 6 shows the dc-link voltage, the grid voltage and current, the grid power and the power factor. The controller regulates the dc link voltage to the reference level. Also, maintains unity power factor and grid voltage/ current are kept in-phase. **The injected active power has a step change according to the change in the wind speed, whereas the reactive power is zero to achieve unity power factor.**

7. CONCLUSIONS

This review paper gives out MPC control strategy for dynamic control of grid-tie WECS. MPPT controller gives out the adjustment of the PMSG rotor speed according to wind speed variation to achieve maximum power at all wind speed.

The MPC has been proven as a good power controller in grid side and torque control is achieved through q-axis current control to achieve rotational speed control of the generator as per wind speed variation. Computer simulations have been carried and results proved that the MPC has accurate tracking performance at different wind speed.

Simulation Results

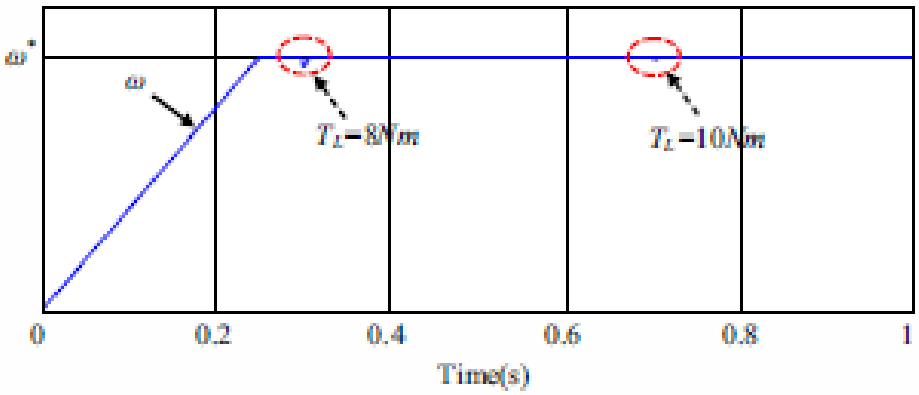

Fig. 7. PMSG Tracking Performance

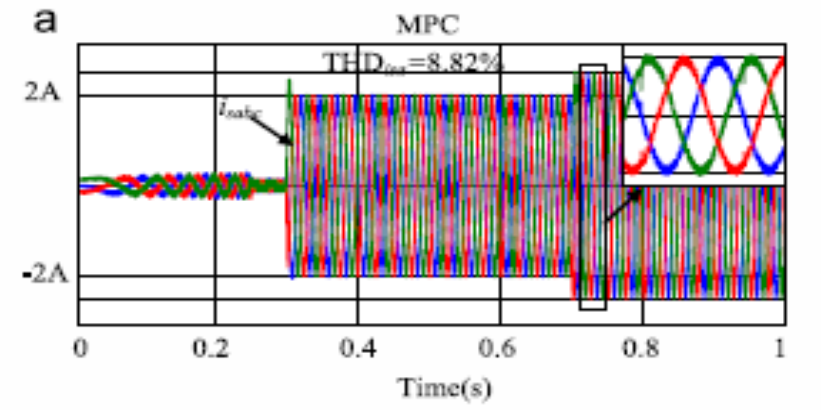

Fig. 8. PMSG Stator Current Waveform

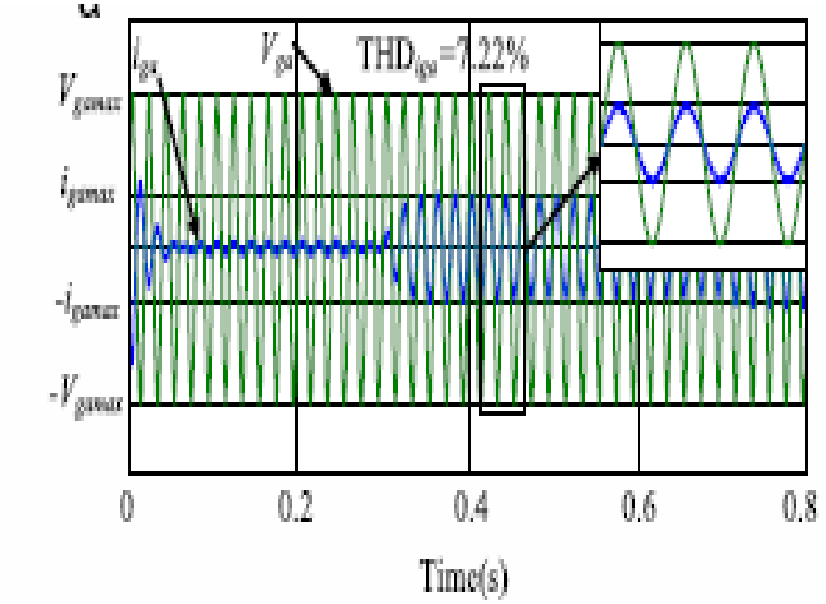

Fig. 9. Grid Voltage and Current Waveform

